Biosensors and Bioelectronics 117 (2018) 224–231

Contents lists available at ScienceDirect

Biosensors and Bioelectronics

journal homepage: www.elsevier.com/locate/bios

A photoelectrochemical aptasensor constructed with core-shell CuS-TiO_2 heterostructure for detection of microcystin-LR

Yunfei Tang[a], Yun Chai[a], Xiaoqiang Liu[a,*], Lele Li[a], Liwei Yang[a], Peipei Liu[a], Yanmei Zhou[a], Huangxian Ju[b,*], Yunzhi Cheng[c]

[a] Henan Joint International Research Laboratory of environmental pollution control materials, College of Chemistry and Chemical Engineering, Henan University, Kaifeng, Henan Province 475004, PR China
[b] State Key Laboratory of Analytical Chemistry for Life Science, Department of Chemistry, Nanjing University, Nanjing 210023, PR China
[c] Journal of Henan University (Medical Science), Henan University, Kaifeng, Henan Province 475004, PR China

ARTICLE INFO

Keywords:
Photoelectrochemical aptasensor
TiO_2 nanospheres
CuS nanoparticles
CuS-TiO_2 heterojunction
Microcystin-LR

ABSTRACT

In this work, a CuS-TiO_2 heterojunction composite was prepared by dispersedly depositing CuS nanoparticles on TiO_2 nanospheres surface with a hydrothermal method, and was then used to construct a photoelectrochemical (PEC) aptasensor for sensitive detection of microcystin-LR (MC-LR) in aquatic environment. The energy bands of CuS nanoparticles and spherical anatase TiO_2 were well matched, which enhanced the photo-to-current conversion efficiency. The composite exhibited the enhanced visible light absorption, the improved separation of photo-generated charges, and the reduced self-aggregation of CuS nanoparticles, leading to the enhanced photocurrent response. The PEC aptasensor was constructed by immobilizing CuS-TiO_2 composite on ITO electrode with chitosan film that further covalently bound aminated aptamer. After the target, microcystin-LR (MC-LR) as an analyte model, was captured by the aptamer on the aptasensor, it could be oxidized by the photo-generated hole to impede the electron-hole recombination and further amplify the photocurrent. The PEC aptasensor showed superior analytical performance for MC-LR with a linear range of 5.0×10^{-5} nM to 250 nM and a detection limit of 2.0×10^{-5} nM. The detection results with the aptasensor for practical water samples indicated its promising application in environmental monitoring.

1. Introduction

As one of the most poisonous microcystins (MCs) produced by cyanobacteria (Murphy et al., 2015; Zhang et al., 2010), microcystin-LR (MC-LR) is considered to be an invisible hepatotoxin, neurotoxin or tumor promoter (Adamovsky et al., 2015). Even at very low concentrations, MC-LR can still inhibit the activity of protein phosphatase (type 2A and type 1) in living cells (Tan et al., 2015) and undermine the homeostasis of protein phosphorylation, resulting in the damage of keratin fibers, liver hemorrhage, hepatitis and primary liver cancer (Zhang et al., 2017). The maximum allowable amount of MC-LR in drinking water was stipulated as 1 $\mu g\,L^{-1}$ by the World Health Organization (Park et al., 2017). Owing to the poor spontaneous degradation and easy accumulation of MC-LR in aquatic ecosystems (Chen et al., 2012), it is necessary to monitor MC-LR in water or aquatic products for the sake of human beings, aquatic organisms and ecological environment. Many methods including high-performance liquid chromatography (HPLC) (Foss and Aubel, 2015), liquid chromatography-mass spectrometry (LC-MS) (Zastepa et al., 2015), capillary electrophoresis (Tong et al., 2010), immunoassay (Hou et al., 2016), and protein phosphatase inhibition assay *etc*. (Sassolas et al., 2011) have been used to detect MC-LR. Nevertheless, these assays always display one or more disadvantages such as complicated and time-consuming operation, large equipment, and cumbersome sample preparation, *etc*. Therefore, it is desirable to develop a fast, highly selective, sensitive and portable technique for detection of MC-LR.

In recent years, photoelectrochemical (PEC) technique has attracted considerable attention in fast and sensitive detection due to its high sensitivity, good stability, fast response, low background noise, and simple instrument needs. In particular, PEC shows high sensitivity due to the capability of transforming optical energy into electrochemical energy, and the complete separation between the excitation source and detection signal (Freeman et al., 2013; Zhao et al., 2016). Furthermore, by combining this technique with biorecognition such as immunoreaction, the developed PEC biosensors can be endowed with high selectivity for specific detections of different analytes (Ju, 2017; Tu

* Corresponding authors.
E-mail addresses: 13781157777@163.com (X. Liu), hxju@nju.edu.cn (H. Ju).

https://doi.org/10.1016/j.bios.2018.06.007
Received 18 April 2018; Received in revised form 29 May 2018; Accepted 4 June 2018
Available online 05 June 2018
0956-5663/

et al., 2012; Wang et al., 2015, 2014; Zang et al., 2017, 2015). As one kind of the newly developing biorecognition elements, DNA aptamers have demonstrated high selectivity to the target analytes (Da et al., 2018; Ho and Leclerc, 2004). In addition, the aptamers also possess many advantages including high stability, low cost, reversible denaturation, and easy functionalization (Yan et al., 2018), and therefore have recently been combined with photoactive materials to develop PEC aptasensors for detection of different targets such as MC-LR (Du et al., 2018), lead (II) (Zang et al., 2014), and 17β-estradiol (Liu et al., 2017a) *etc*. For example, PEC aptasensors for MC-LR were developed by immobilizing MC-LR aptamer on different photoactive materials (Liu et al., 2015, 2017b) such as BiOBr nanoflakes/N-doped graphene heterojunction electrode (Du et al., 2016). Although these aptasensors exhibited acceptable performances, their sensitivities are relatively low, probably ascribed to the weak PEC response from the photoactive materials.

To further improve the performance of PEC biosensors, different semiconductors with matched energy levels have been hybridized to achieve high photo-to-current conversion efficiency for greatly increasing the PEC properties (Zang et al., 2017). For example, CdS/PPy/g-C_3N_4 nanocomposite was used to construct a PEC aptasensor for adenosine (Liu et al., 2016b). Due to the restriction of PPy/g-C_3N_4 on the self-oxidation of CdS and the recombination of photo-generated charges, the photo-to-current conversion efficiency of the nanocomposite was greatly enhanced, and the aptasensor showed wide linear range and low detection limit. Besides CdS nanoparticles, copper sulfide (CuS) is also sensitive to the visible light excitation due to its narrow bandgap of ~2.1 eV, which has thus been used in solar cells, optical filter, infrared detectors, sensors and photocatalysis *etc*. (Zou et al., 2007). However, sole CuS in nano-morphology is easily subjected to the serious aggregation (Nie et al., 2013), which greatly undermines its PEC properties. Fortunately, this drawback can be alleviated by combining CuS with the suitable co-catalysts. For example, CuS nanoparticles were dispersedly deposited on reduced graphene oxide to form a nanocomposite by a simple microwave irradiation method, which was used as a photocatalyst for degrading diazo CR dye molecules (Borthakur et al., 2016). Furthermore, the well matched energy bands between the two nanomaterials also facilitated the separation of the photo-generated charges and increased the photocurrent response to visible light excitation.

To develop sensitive PEC aptasensor for MC-LR detection, this work designed a CuS-TiO_2 heterojunction composed of CuS nanoparticles and spherical anatase TiO_2. The CuS nanoparticles were uniformly deposited on the surface of TiO_2 nanospheres by a hydrothermal method, which greatly alleviated the self-aggregation of CuS. The well matched energy bands between the two nanomaterials enhanced the visible light absorption and improved the separation of photo-generated charges, significantly increasing the photo-to-current conversion efficiency. After the CuS-TiO_2 nanocomposite was immobilized on ITO with chitosan film, the PEC aptasensor was fabricated by using glutaraldehyde as a linker to covalently bind corresponding aminated aptamer to chitosan film. The proposed PEC aptasensor showed high specificity, sensitivity, stability and low detection limit for the detection of MC-LR.

2. Experimental

2.1. Material and reagents

All reagents were of analytical grade and used without further purification. ITO electrodes (10 mm × 20 mm × 1.1 mm, resistivity 8 Ω) were obtained from Wuhan Lattice Solar Energy Technology, Ltd., China. Microcystin-LR, microcystin-LA (MC-LA) and microcystin-YR (MC-YR) were supplied by MedChemExpress, China. Atrazine, trichlorfon, bovine serum albumin (BSA) and absolute ethanol were purchased from Sinopharm Chemical Reagent Co., Ltd., China. Potassium chloride and copper (II) chloride dihydrate were obtained from Kermel Chemical Reagent Co., Ltd., China. Titanium (IV) isopropoxide (TIP, 97 + %) was acquired from Alfa Aesar (China) Chemical Co., Ltd. Hexadecylamine (HDA, 90%), L-cysteine (99%), chitosan (85% deacetylation) and glutaraldehyde (50%) were obtained from Aladdin Reagent Co., Ltd., China. Phosphate buffer solution (PBS, pH 7.4) consisting of 0.1 M KH_2PO_4, K_2HPO_4 and KCl was prepared as the supporting electrolyte. The ultrapure water (≥18 MΩ cm^{-1}) made from a Millipore water purification system was used throughout the whole experiment. The aminated MC-LR aptamer was purchased from Shanghai Sangon Biotechnology Co. Ltd. (Shanghai, China) with the following sequences: 5′-NH_2-$(CH_2)_6$-GGC GCC AAA CAG GAC CAC CAT GAC AAT TAC CCA TAC CAC CTC ATT ATG CCC CAT CTC CGC-3′

2.2. Apparatus

The PEC measurements were performed at a CHI630D electrochemical workstation (CH Instruments, Shanghai, China) in a conventional three-electrode cell containing 0.1 M PBS and 0.1 M KCl solution with Ag|AgCl (3.0 M KCl) as reference electrode and platinum wire as counter electrode. A Xe lamp equipped with a 400 nm cut-off filter was used as the visible light source (CEL-HXUV 300, Beijing AULTT, China). Electrochemical impedance spectroscopy (EIS) was performed on an IM6ex electrochemical analyzer (Zahner, Germany) in 0.1 M KCl solution containing 5.0 mM $[Fe(CN)_6]^{3-/4-}$ within a frequency range of 100 kHz-0.1 Hz at 0.23 V. The morphologies of the materials were obtained by field emission scanning electron microscopy (SEM, JSM-7500F, JEOL., Japan). The crystal form and element composition were investigated by X-ray powder diffraction (XRD, X-Pert Pro, Netherland) with Cu Kα radiation (λ = 1.5406 nm), and X-ray photoelectron spectrometer (XPS, ESCALAB 250Xi, USA) with a monochromated Al Kα source (hν = 1486.6 eV, 150 W power, and 500 μm beam spot). The spectra were calibrated on the C 1 s peak (284.8 eV) and analyzed by XPSPEAK41 software. UV–vis diffuse reflectance spectra were acquired at an UV–vis spectrophotometer (DRS, UV-2600, Kyoto, Japan).

2.3. Synthesis of CuS-TiO_2 composite

Initially, spherical TiO_2 was prepared according to a previous report with slight modification (Tubío et al., 2015). Firstly, 0.4375 g HDA was dissolved in 50 mL of ethanol, followed by the addition of 0.2 mL of KCl solution (0.1 M) and 127.5 μL of ultrapure water. After 5 min of stirring, 1.08 mL of TIP was added to the above solution and the mixture was stirred for 40 min. Then the mixture was left still for 18 h before it was centrifuged, washed with ethanol and dried at 60 °C for 8 h. Subsequently, the resulting sample was calcined at 450 °C for 2 h to obtain anatase TiO_2.

CuS-TiO_2 composite was synthesized by the hydrothermal method. Initially, 0.0719 g of anatase TiO_2 was dispersed in 36 mL of ultrapure water, and 145.2 mg of L-cysteine was then added to the above suspension. After 30 min of ultrasonic, 3 mL of $CuCl_2$ solution (0.1 M) was dropwise added to the suspension over 20 min. Subsequently, the reaction solution was stirred for 30 min before it was transferred to a 100 mL Teflon-lined stainless steel autoclave and maintained at 160 °C for 12 h. The obtained product was washed three times with ultrapure water and ethanol, and dried at 60 °C overnight.

2.4. Fabrication of PEC aptasensor

The fabrication of the proposed PEC aptasensor is elaborated in Scheme 1. Firstly, ITO conductive glass was successively washed in toluene, acetone, ethanol and ultrapure water with 15 min ultrasonic, and dried in air. Meanwhile, 2 mg of CuS-TiO_2 nanocomposite was dispersed in 1 mL of 0.2% chitosan solution (in 1% w/v acetic acid) to obtain a uniform suspension. A droplet (20 μL) of CuS-TiO_2 suspension was then cast to the surface of cleaned ITO with a fixed area of 0.5 cm^2 and dried at room temperature. Afterward, the CuS-TiO_2|ITO was

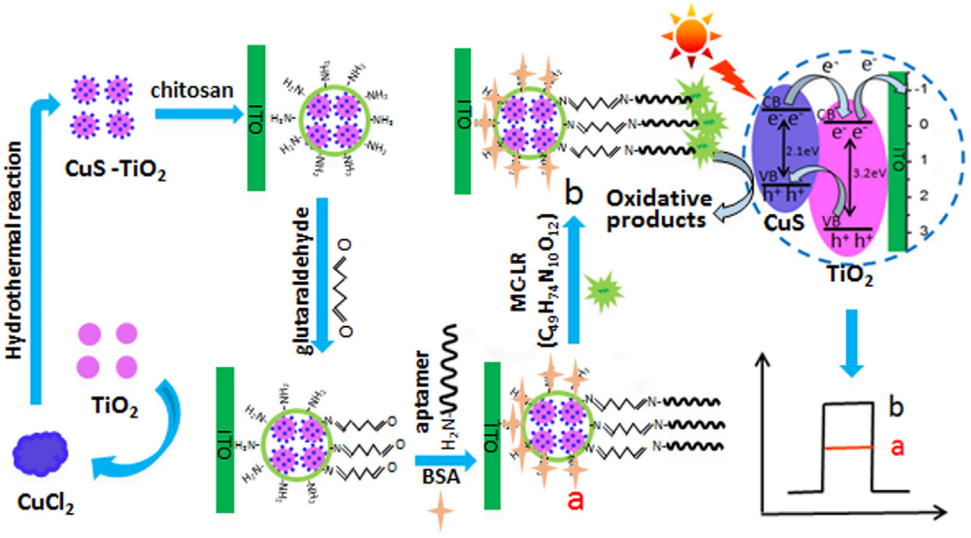

Scheme 1. Schematic diagram of the assembly and PEC mechanism of the aptasensor.

immersed in 2.5% glutaraldehyde for 30 min, and then washed with ultrapure water. The glutaraldehyde-functionalized CuS-TiO_2|ITO was then coated with 20 μL of aminated MC-LR aptamer (2.5 μM) for 3 h to obtain aptamer|CuS-TiO_2|ITO, which was rinsed with PBS to remove unbound aptamer and treated with 10 μL of 3% (w/v) BSA for 30 min to block the non-specifically bound active sites. Finally, the PEC aptasensor was washed with PBS to remove excess BSA and stored at 4 °C for later use.

3. Results and discussion

3.1. Morphological characterization of nanomaterials

The morphologies of TiO_2 nanospheres, CuS nanoparticles and CuS-TiO_2 nanocomposites are displayed in Fig. 1. The TiO_2 nanospheres showed the well separated and smooth morphology with a uniform diameter of ~360 nm (Fig. 1A), while CuS nanoparticles were seriously self-aggregated in the absence of other nanomaterials and their morphologies were hardly to be distinguished (Fig. 1B). From the SEM images of CuS-TiO_2 composite (Fig. 1C and D), it could be clearly seen that smooth TiO_2 nanospheres were densely covered with separated CuS nanoparticles. The diameter of CuS-TiO_2 composite was slightly larger than that of TiO_2 nanospheres, ascribed to the presence of CuS on TiO_2. The above micrographs revealed that CuS-TiO_2 heterojunction was successfully prepared and the formation of the composite effectively reduced the aggregation of CuS nanoparticles.

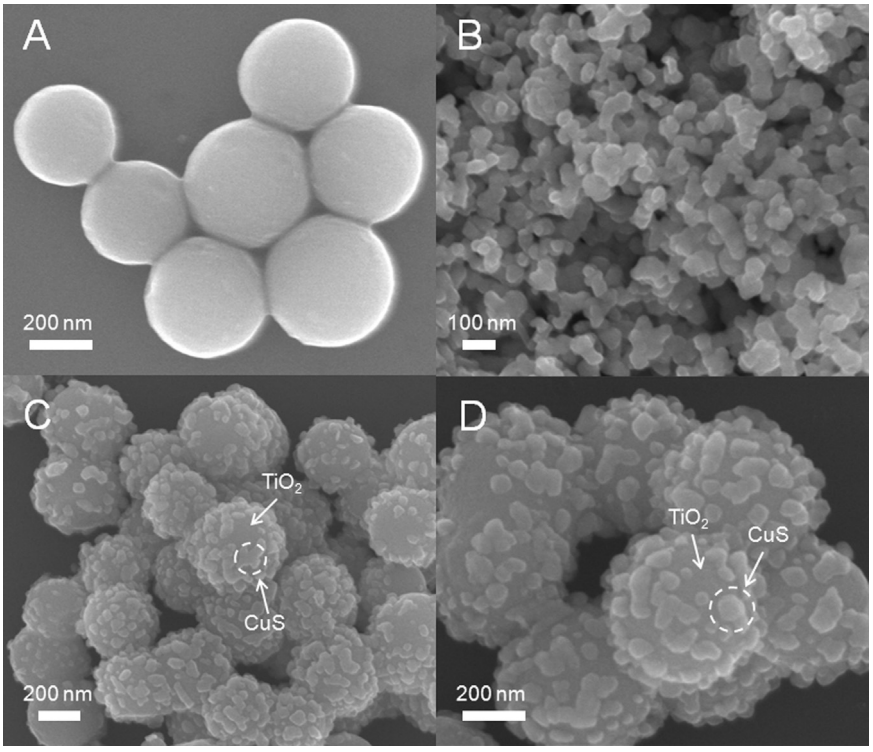

Fig. 1. SEM images of (A) TiO_2 nanospheres, (B) CuS nanoparticles, (C) and (D) CuS-TiO_2 composite at different magnifications.

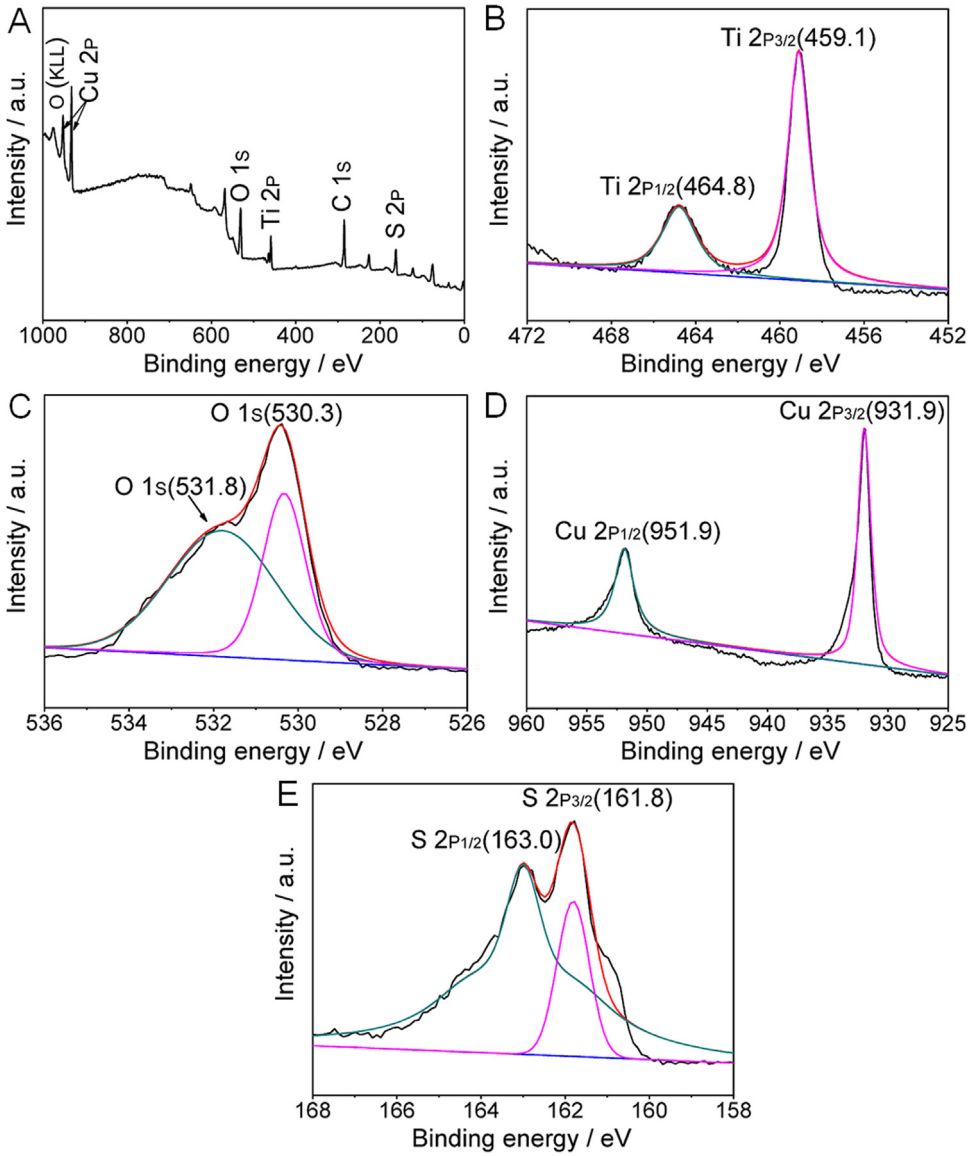

Fig. 2. XPS analysis of CuS-TiO_2 composite: (A) survey scans, and high-resolution spectra of (B) Ti 2p, (C) O 1 s, (D) Cu 2p and (E) S 2p.

3.2. XPS characterization of nanomaterials

XPS technology is regarded as one of the most effective methods to obtain the chemical composition, purity, and electronic state of various nanomaterials. The survey spectrum of the CuS-TiO_2 composite (Fig. 2A) presented all the Ti, O, Cu, S and C element peaks (Li et al., 2017), and O KLL Auger peak at 976 eV (Zong et al., 2014). The XPS high-resolution spectrum of Ti 2p showed two peaks at 459.1 and 464.8 eV (Fig. 2B), assigned to Ti $2p_{3/2}$ and Ti $2p_{1/2}$ of Ti^{4+} in TiO_2, respectively (Wang et al., 2013). In Fig. 2C, the peaks of O 1 s at 530.3 and 531.8 eV were attributed to lattice oxygen [Ti-O_6] in anatase TiO_2 and hydroxyl oxygen in Ti-OH, respectively, indicating that the existence state of O was O^{2-} in the composite (Lu et al., 2016; Yang et al., 2014). Two peaks at ~931.9 eV and 951.9 eV in Fig. 2D could be ascribed to Cu $2p_{3/2}$ and Cu $2p_{1/2}$ in Cu^{2+} state (Chen et al., 2016). The two peaks of S $2p_{3/2}$ and S $2p_{1/2}$ located at 161.8 and 163.0 eV respectively in Fig. 2E indicated the S^{2-} state in the composite (Chen et al., 2017; Manjunath et al., 2016). In summary, it is concluded that Ti, O, Cu and S exist as Ti^{4+}, O^{2-}, Cu^{2+} and S^{2-} in the composite, respectively, which further indicates the successful preparation of CuS-TiO_2 composite.

3.3. XRD and UV–vis diffuse reflectance spectra of nanomaterials

The crystalline structure of the prepared nanomaterials was analyzed by X-ray powder diffraction as shown in Fig. 3A. The diffraction peaks at 25.33°, 37.84°, 48.01°, 54.26°, 54.75° and 62.68° (curve a) corresponded to (101), (004), (200), (105), (211) and (204) crystal faces, respectively, which was consistent with the standard caliper of anatase TiO_2 (JCPDS No. 21-1272) (Yang et al., 2014). The diffraction peaks of TiO_2 were tall and sharp and no other impurity peak was observed, indicating the high purity of synthesized anatase TiO_2. The diffraction peaks at 27.68°, 29.30°, 31.77°, 32.85°, 38.92°, 47.95°, 52.82° and 59.37° (curve b), attributed to (101), (102), (103), (006), (105), (110), (108) and (116) crystal faces respectively, coincided with the peaks of hexagonal CuS (JCPDS No. 06–0464) (Gao et al., 2017). Most importantly, the peaks from both anatase TiO_2 and CuS were present in XRD pattern of CuS-TiO_2 composite (curve c), demonstrating the successful deposition of CuS on TiO_2.

Fig. 3B displays the absorbance of the nanomaterials obtained by UV–vis diffuse reflectance spectroscopy (DRS). The absorption edge of anatase TiO_2 is located at ~388.5 nm (curve a), confirming its poor visible light absorption. According to Scherer equation: $E_g = 1240 / \lambda$,

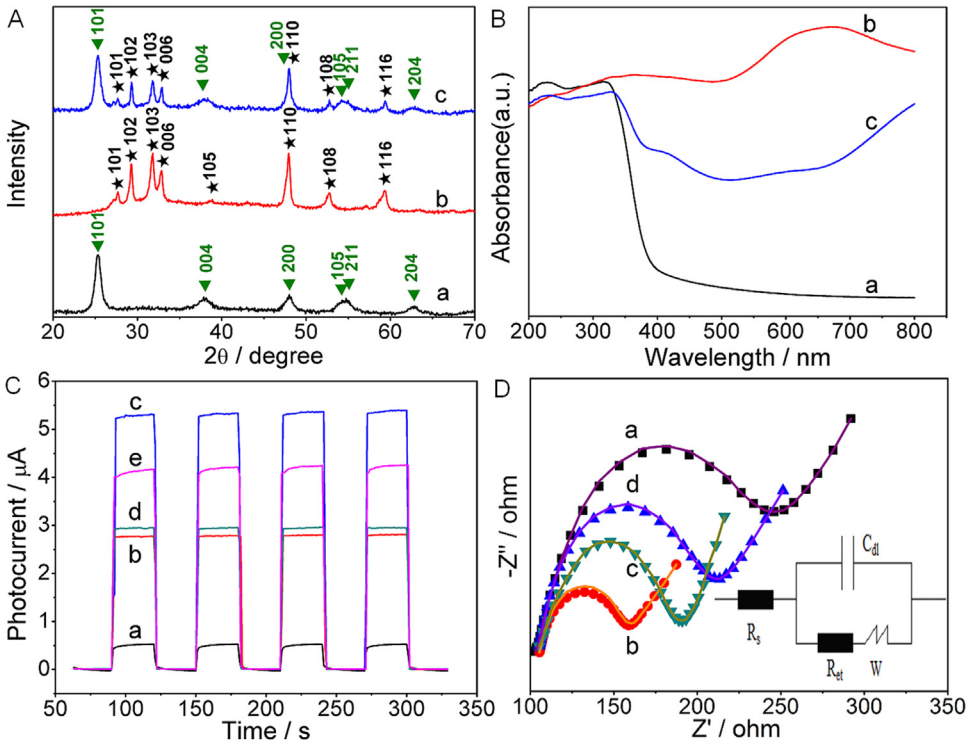

Fig. 3. (A) XRD patterns and (B) DRS of (a) TiO_2 nanospheres, (b) CuS nanoparticles and (c) CuS-TiO_2 composite. (C) Photocurrent response of (a) TiO_2|ITO, (b) CuS|ITO, (c) CuS-TiO_2|ITO, (d) BSA|aptamer|CuS-TiO_2|ITO and (e) MC-LR (0.1 nM) |BSA|aptamer|CuS-TiO_2|ITO in 0.1 M PBS (pH 7.4) containing 0.1 M KCl at an applied potential of 0.1 V. (D) EIS of (a) TiO_2|ITO, (b) CuS-TiO_2|ITO, (c) aptamer|CuS-TiO_2|ITO and (d) BSA|aptamer|CuS-TiO_2|ITO in 0.1 M KCl containing 5 mM $[Fe(CN)_6]^{3-/4-}$.

the bandgap energy (E_g) is inversely proportional to the absorption edge wavelength of λ (Liu et al., 2017a). Owing to the narrow bandgap of ~2.1 eV, the theoretical absorption edge of pure CuS is calculated to be ~590 nm from the Scherer equation. However, the actual absorption of CuS has extended to the near-infrared region (> 700 nm) (curve b), attributed to the local surface plasmonic resonance that resulted from the collective oscillation of Cu defect-induced free carriers on CuS nanoparticles (Chen et al., 2016). Therefore, pure CuS exhibits the strong absorption in both UV and visible light region between 300 nm and 700 nm. The absorption edge of CuS-TiO_2 composite is estimated to be ~504 nm from curve c, which is much longer than that of pure TiO_2, demonstrating that CuS-TiO_2 heterojunction significantly improved the visible light absorption of TiO_2.

3.4. Characterization of PEC aptasensor

To verify the photoelectric properties of the materials and the feasibility of the prepared PEC aptasensor for the detection of MC-LR, the photocurrent responses of TiO_2|ITO, CuS|ITO, CuS-TiO_2|ITO, BSA|aptamer|CuS-TiO_2|ITO were evaluated under intermittent visible light irradiation (Fig. 3C). The weak photocurrent signal of TiO_2|ITO (curve a) was due to the large bandgap and the easy electron-hole recombination of TiO_2. Despite of the narrow bandgap of CuS, the photocurrent at CuS|ITO was only slightly larger than that at TiO_2|ITO, most likely due to the serious self-aggregation of CuS nanoparticles (curve b). In contrast to CuS|ITO, CuS-TiO_2 composite produced the largest photocurrent response among all the photoelectrodes, ascribed to the well matched energy levels between CuS and TiO_2 (curve c). As shown in Scheme 1, both the conduction band (CB) and the valence band (VB) levels of CuS were higher than those of TiO_2. Accordingly, the generated photoelectrons of CuS tended to migrate toward the lower CB of TiO_2, while the photo-generated holes on TiO_2 also moved to the higher VB of CuS, promoting the charge separation and thereby increasing the photocurrent (Khanchandani et al., 2016). After MC-LR aptamer was bound on CuS-TiO_2|ITO electrode, the photocurrent decreased (curve d) because the steric hindrance of biomolecules on the electrode interface inhibited the electron transfer and increased the recombination between electrons and holes. Because the oxidation potential of MC-LR (+0.2 V) (Du et al., 2018) was much smaller than the VB energy (1.6 V) of the holes, the MC-LR trapped by the aptasensor could be easily oxidized by the holes, hindering the electrons-hole recombination. Therefore, the photocurrent response was amplified in the presence of MC-LR as displayed in curve e.

To assess the electron transfer at the electrode surface during the aptasensor assembly, the EIS test was performed using $[Fe(CN)_6]^{3-/4-}$ as a redox probe. As shown in inset of Fig. 3D, the equivalent circuit is composed of the resistance of solution (R_s), the double layer capacitance (C_{dl}), the electron transfer resistance (R_{et}) and the Warburg impedance (Z_W). The high frequency semicircle in the Nyquist plot represents the R_{et}, which can reflect the immobilization situation on the modified electrode interface (Fan et al., 2016). The Nyquist plot at CuS-TiO_2|ITO showed a much smaller half-circle diameter than TiO_2|ITO (Fig. 3D, curve b and a), possibly because CuS improved the electron transfer of $[Fe(CN)_6]^{3-/4-}$ at the electrode surface. The R_{et} at aptamer|CuS-TiO_2|ITO was significantly larger than that at CuS-TiO_2|ITO (Fig. 3D, curves c and b), indicating the successful immobilization of aptamer on the composite modified ITO surface. The loading of BSA on aptamer|CuS-TiO_2|ITO (curve d) further impeded the electron exchange at the electrode surface, resulting in the increase of R_{et}. The impedance results demonstrated the successive immobilization of different components on the ITO electrode. Subsequently, the electrochemical impedance data was fitted according to the equivalent circuit in the inset of Fig. 3D and the fitted results (solid lines) were basically the same as the measured plots (dotted lines).

3.5. Optimization of experimental conditions

To improve the PEC aptasensor performance, we optimized several relevant experimental conditions including aptamer concentration, incubation time of the aptamer on the electrode, pH of the test solution and applied potential. The photocurrent response increased with increasing aptamer concentration from 0.5 μM to 2.5 μM (Fig. 4A) probably because higher concentration of aptamer could capture more MC-LR molecules to produce larger photocurrent. When the aptamer

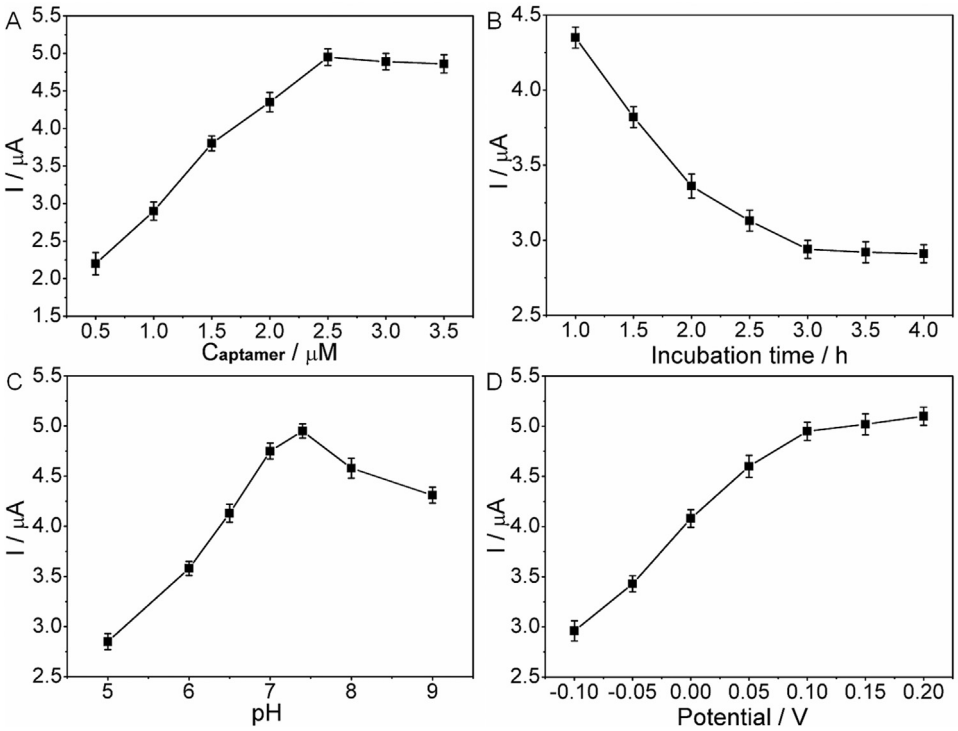

Fig. 4. Effects of (A) aptamer concentration, (B) incubation time of aptamer on the electrode, (C) pH of test solution, and (D) applied potential on photocurrent of the resulting aptamer in 0.1 M PBS (pH 7.4) containing 0.1 M KCl and 50 nM MC-LR.

concentration reached 2.5 μM, the photocurrent exhibited a downward tendency, possibly because high concentration of the aptamer produced strong steric hindrance to impede electron transfer. Therefore, 2.5 μM was selected as the optimal concentration of aptamer concentration, at which the photocurrent almost reached a plateau at the incubation time of 3 h (Fig. 4B), indicating saturated linkage of aptamer on the electrode surface.

The photocurrent continued to increase with the increasing pH of test solution from 5 to 7.4, and reached the maximum value at pH 7.4 (Fig. 4C). Afterward the photocurrent reduced, suggesting that the binding of MC-LR to the aptamer was weakened in alkaline solution. This was attributed that both the protonation of the aptamer guanine groups at pH $<$ 7.0 and the negative charge increase of the aptamer at pH $>$ 8.0, which might destroy the structure of the aptamers and eventually inactivated them (Zhao et al., 2011). The photocurrent presented a fast rising tendency with the increasing applied potential and became nearly flat after the potential exceeded 0.1 V (Fig. 4D). This is due to the fact that the increased potential facilitated the separation of the photo-generated electron-hole pairs, leading to the large photocurrent. Considering that low potential can minimize the interference from other coexisting species in the sample (Liu et al., 2016a), an applied potential of 0.1 V was chosen for the subsequent PEC test.

3.6. Performance of PEC aptasensor

Under the optimal conditions, the PEC aptasensor was applied for the quantitative determination of MC-LR. The photocurrent increased with the increasing MC-LR concentration from 5.0×10^{-5} nM to 250 nM (Fig. 5A), which resulted from the consumption of the holes by MC-LR to facilitate electron-hole separation. The photocurrent change ($\Delta I = I - I_0$) was directly proportional to the logarithm of MC-LR concentration from 5.0×10^{-5} nM to 250 nM with a correlation coefficient of 0.993 and a detection limit of 2.0×10^{-5} nM (S/N = 3) (inset in Fig. 5A). The proposed aptasensor displayed a wider linear range and lower detection limit due to the special features of CuS-TiO_2 composite, compared with previous reported sensors (Table S1). For example, it displayed a comparable detection limit and relatively wider dynamic range for MC-LR detection than the PEC sensing platform based on AgI-nitrogen-doped graphene (AgI-NG) composites (Du et al., 2018). The improved performance of the proposed sensor was due to the large specific surface and good biocompatibility, excellent photoelectric conversion ability and strong visible light absorption of the composite.

3.7. Stability, reproducibility and specificity of the PEC aptasensor

The photo-excitation “on-off-on” alternating signals remained nearly stable both in the presence and absence of MC-LR (Fig. 3C, curves e and d), demonstrating the good short term stability of the proposed aptasensor. In addition, the photocurrent response at the PEC aptasensor retained ~91.8% of the initial value after it was placed in a 4 °C refrigerator for 10 days, revealing the acceptable long term stability of the aptasensor. The reproducibility of the aptasensor was obtained by testing five identical sensors in the same experimental conditions. A relative standard deviation (RSD) of 5.3% was obtained, showing the possible application prospect of the aptasensor. The specificity of the aptasensor was judged by comparing the photocurrent change (ΔI) after applying 10 nM of various interferents on the aptasensor. These interferents included two homologues (MC-LA and MC-YR) with the similar structures to MC-LR and the possible contaminants in the water such as atrazine and trichlorfon. The photocurrent change caused by MC-LR was overwhelmingly larger than those by the other four interferents (Fig. 5B), indicating the high specificity of the aptasensor to MC-LR.

3.8. Real sample analysis of the PEC aptasensor

To further evaluate the accuracy and practical application of the aptasensor under the interference of the composite substrates, the amounts of MC-LR in practical samples such as lake water, river water and tap water were studied respectively. Before the test, the collected water samples were centrifuged at 4000 r min^{-1} for 10 min to remove the large suspended matter. Then, small particles and suspended solids

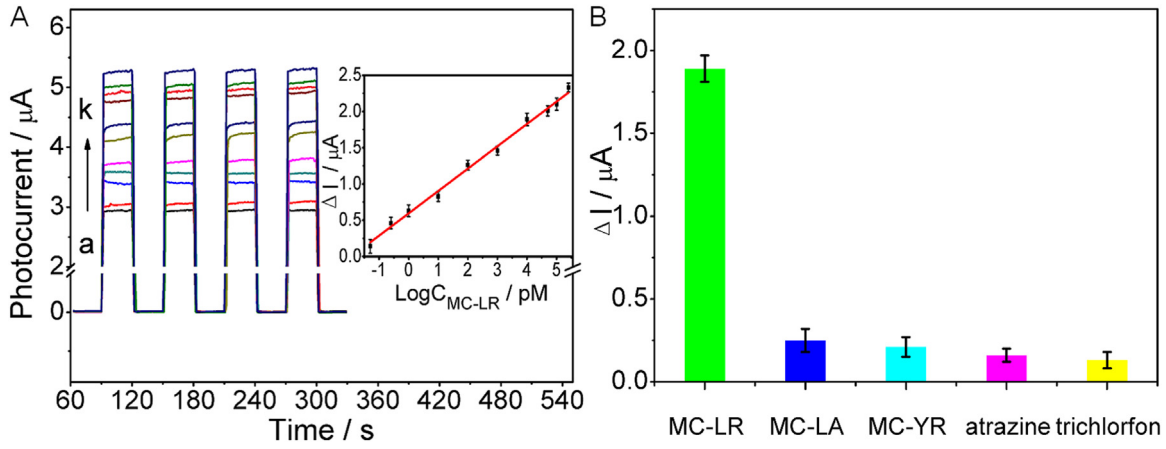

Fig. 5. (A) Photocurrent responses of the aptasensor at different concentrations of MC-LR (from a to k: 0, 5.0 $\times 10^{-5}$, 2.5 $\times 10^{-4}$, 1.0 $\times 10^{-3}$, 1.0 $\times 10^{-2}$, 0.1, 1.0, 10, 50, 100 and 250 nM) in 0.1 M PBS (pH 7.4) containing 0.1 M KCl at an applied potential of 0.1 V. Inset: Plot of photocurrent change (ΔI) vs. Log $C_{MC\text{-}LR}$. (B) Photocurrent changes (ΔI) after incubating the aptasensor with 10 nM MC-LR, MC-LA, MC-YR, atrazine and trichlorfon. Error bars represent the standard deviations of measurements taken from four independent experiments.

were removed through filter paper and 0.22 μm membrane, which reduced the signal interference and increased the sensitivity and accuracy of the aptasensor. The initial concentrations of MC-LR in the three water samples were obtained by routine HPLC technique and the PEC aptasensor was subsequently tested using the standard addition method. In this method, different volumes of concentrated MC-LR standard solutions were added into the water samples to the final concentrations of 0.3, 0.4 and 0.5 nM respectively. The recovery ranging from 93.4% to 106.3% (Table S2) indicated the potential of the sensor for the detection of MC-LR in environmental water samples.

4. Conclusion

This work designs a novel CuS-TiO_2 heterojunction with well-matched energy bands between the two nanomaterials by uniformly depositing CuS nanoparticles on the surface of TiO_2 nanospheres with a hydrothermal method for construction of a PEC MC-LR aptasensor. The successful synthesis of the nanocomposite not only improves the visible absorption efficiency of TiO_2 and the separation of photo-generated charges, but also alleviates the self-aggregation of CuS, which leads to the enhanced photocurrent response. The composite also possesses a large specific surface and good biocompatibility for loading significant amount of aptamer and retaining their bioactivity. Attributed to these features of the composite, the proposed aptasensor shows an ultrasensitive PEC detection of MC-LR with a wide linear range, a detection limit down to 2.0 $\times 10^{-5}$ nM, high specificity, good stability and reproducibility. Although the preparation time of the aptasensor is little long, these results demonstrates the feasibility of CuS-TiO_2 heterojunction for developing various aptasensors.

Acknowledgments

This work was financially supported by National Natural Science Foundation of China (No. U1504215, 21576071, 21776061) and International Science and Technology Cooperative Project funded by The Department of Science and Technology of Henan Province (172102410042).

Appendix A. Supporting information

Supplementary data associated with this article can be found in the online version at http://dx.doi.org/10.1016/j.bios.2018.06.007.

References

Adamovsky, O., Moosova, Z., Pekarova, M., Basu, A., Babica, P., Svihalkova Sindlerova, L., Kubala, L., Blaha, L., 2015. Environ. Sci. Technol. 49, 12457–12464.
Borthakur, P., Boruah, P.K., Darabdhara, G., Sengupta, P., Das, M.R., Boronin, A.I., Kibis, L.S., Kozlova, M.N., Fedorov, V.E., 2016. J. Environ. Chem. Eng. 4, 4600–4611.
Chen, K., Liu, M., Zhao, G., Shi, H., Fan, L., Zhao, S., 2012. Environ. Sci. Technol. 46, 11955–11961.
Chen, Q., Wu, S., Xin, Y., 2016. Chem. Eng. J. 302, 377–387.
Chen, T., Song, C., Fan, M., Hong, Y., Hu, B., Yu, L., Shi, W., 2017. Int. J. Hydrog. Energy 42, 12210–12219.
Da, H., Liu, H., Zheng, Y., Yuan, R., Chai, Y., 2018. Biosens. Bioelectron. 101, 213–218.
Du, X., Jiang, D., Dai, L., Zhou, L., Hao, N., Qian, J., Qiu, B., Wang, K., 2016. Biosens. Bioelectron. 81, 242–248.
Du, X., Jiang, D., Li, H., Hao, N., You, T., Wang, K., 2018. Sens. Actuators, B 259, 316–324.
Fan, D., Guo, C., Ma, H., Zhao, D., Li, Y., Wu, D., Wei, Q., 2016. Biosens. Bioelectron. 75, 116–122.
Foss, A.J., Aubel, M.T., 2015. Toxicon 104, 91–101.
Freeman, R., Girsh, J., Willner, I., 2013. ACS Appl. Mater. Interfaces 5, 2815–2834.
Gao, L., Du, J., Ma, T., 2017. Ceram. Int. 43, 9559–9563.
Ho, H.-A., Leclerc, M., 2004. J. Am. Chem. Soc. 126, 1384–1387.
Hou, L., Ding, Y., Zhang, L., Guo, Y., Li, M., Chen, Z., Wu, X., 2016. Sens. Actuators, B 233, 63–70.
Ju, H., 2017. J. Anal. Test. 1, 7.
Khanchandani, S., Kumar, S., Ganguli, A.K., 2016. ACS Sustain. Chem. Eng. 4, 1487–1499.
Li, L., Ya, J., Xiang, L., Liu, Z., Lei, E., 2017. Appl. Phys. A: Mater. Sci. Process. 123, 667.
Liu, M., Yu, J., Ding, X., Zhao, G., 2015. Electroanalysis 28, 161–168.
Liu, P.P., Liu, X., Huo, X.H., Tang, Y., Xu, J., Ju, H., 2017a. ACS Appl. Mater. Interfaces 9, 27185–27192.
Liu, Q., Huan, J., Dong, X., Qian, J., Hao, N., You, T., Mao, H., Wang, K., 2016a. Sens. Actuators, B 235, 647–654.
Liu, Q., Huan, J., Hao, N., Qian, J., Mao, H., Wang, K., 2017b. ACS Appl. Mater. Interfaces 9, 18369–18376.
Liu, Y., Ma, H., Zhang, Y., Pang, X., Fan, D., Wu, D., Wei, Q., 2016b. Biosens. Bioelectron. 86, 439–445.
Lu, Y.Y., Zhang, Y.Y., Zhang, J., Shi, Y., Li, Z., Feng, Z.C., Li, C., 2016. Appl. Surf. Sci. 370, 312–319.
Manjunath, K., Souza, V.S., Nagaraju, G., Marcos Leite Santos, J., Dupont, J., Ramakrishnappa, T., 2016. New J. Chem. 40, 10172–10180.
Murphy, C., Stack, E., Krivelo, S., McPartlin, D.A., Byrne, B., Greef, C., Lochhead, M.J., Husar, G., Devlin, S., Elliott, C.T., O'Kennedy, R.J., 2015. Biosens. Bioelectron. 67, 708–714.
Nie, G., Zhang, L., Lu, X., Bian, X., Sun, W., Wang, C., 2013. Dalton Trans. 42, 14006–14013.
Park, J.-A., Jung, S.-M., Yi, I.-G., Choi, J.-W., Kim, S.-B., Lee, S.-H., 2017. Chemosphere 177, 15–23.
Sassolas, A., Catanante, G., Fournier, D., Marty, J.L., 2011. Talanta 85, 2498–2503.
Tan, F., Saucedo, N.M., Ramnani, P., Mulchandani, A., 2015. Environ. Sci. Technol. 49, 9256–9263.
Tong, P., Zhang, L., He, Y., Tang, S., Cheng, J., Chen, G., 2010. Talanta 82, 1101–1106.
Tu, W., Wang, W., Lei, J., Deng, S., Ju, H., 2012. Chem. Commun. 48, 6535–6537.
Tubío, C.R., Guitián, F., Salgueiro, J.R., Gil, A., 2015. Mater. Lett. 141, 203–206.
Wang, G.-L., Shu, J.-X., Dong, Y.-M., Wu, X.-M., Li, Z.-J., 2015. Biosens. Bioelectron. 66, 283–289.
Wang, Q., An, N., Bai, Y., Hang, H., Li, J., Lu, X., Liu, Y., Wang, F., Li, Z., Lei, Z., 2013. Int.

J. Hydrog. Energy 38, 10739–10745.
Wang, W., Hao, Q., Wang, W., Bao, L., Lei, J., Wang, Q., Ju, H., 2014. Nanoscale 6, 2710–2717.
Yan, X., Li, J., Yang, R., Li, Y., Zhang, X., Chen, J., 2018. Sens. Actuators, B 255, 2187–2193.
Yang, K., Huang, K., He, Z., Chen, X., Fu, X., Dai, W., 2014. Appl. Catal., B 158–159, 250–257.
Zang, Y., Lei, J., Hao, Q., Ju, H., 2014. ACS Appl. Mater. Interfaces 6, 15991–15997.
Zang, Y., Lei, J., Ju, H., 2017. Biosens. Bioelectron. 96, 8–16.
Zang, Y., Lei, J., Ling, P., Ju, H., 2015. Anal. Chem. 87, 5430–5436.
Zastepa, A., Pick, F.R., Blais, J.M., Saleem, A., 2015. Anal. Chim. Acta 872, 26–34.
Zhang, J., Lei, J., Xu, C., Ding, L., Ju, H., 2010. Anal. Chem. 82, 1117–1122.
Zhang, W., Han, C., Jia, B., Saint, C., Nadagouda, M., Falaras, P., Sygellou, L., Vogiazi, V., Dionysiou, D.D., 2017. Electrochim. Acta 236, 319–327.
Zhao, J., Zhang, Y., Li, H., Wen, Y., Fan, X., Lin, F., Tan, L., Yao, S., 2011. Biosens. Bioelectron. 26, 2297–2303.
Zhao, P., Li, D., Yao, S., Zhang, Y., Liu, F., Sun, P., Chuai, X., Gao, Y., Lu, G., 2016. J. Power Sources 318, 49–56.
Zong, M., Huang, Y., Wu, H., Zhao, Y., Wang, Q., Sun, X., 2014. Mater. Lett. 114, 52–55.
Zou, J., Zhang, J., Zhang, B., Zhao, P., Xu, X., Chen, J., Huang, K., 2007. J. Mater. Sci. 42, 9181–9186.